Mapping Electron Beam-Induced Radiolytic Damage in Molecular Crystals

Ambarneil Saha[1*], Matthew Mecklenburg[2], Alexander Pattison[1], Aaron Brewster[3], Jose A. Rodriguez[1*], and Peter Ercius[2*]

[1]National Center for Electron Microscopy, Molecular Foundry, Lawrence Berkeley National Laboratory, Berkeley, California 94720, United States
[2]California NanoSystems Institute, University of California, Los Angeles, California 90095, United States
[3]Molecular Biophysics and Integrated Bioimaging Division, Lawrence Berkeley National Laboratory, Berkeley, California 94720, United States
[4]Department of Chemistry and Biochemistry, University of California, Los Angeles, California 90095, United States

*Corresponding authors: asaha2@lbl.gov, jrodriguez@mbi.ucla.edu, percius@lbl.gov

Every electron crystallography experiment is fundamentally limited by radiation damage. Immediately as a molecular crystal is illuminated within a transmission electron microscope, it undergoes sustained bombardment with extremely damaging levels of ionizing radiation [1]. Electrons accelerated to relativistic speeds typically deposit quantities of energy per unit mass in the range of megagrays (MGy; 10^6 J kg^{-1}) [2] several orders of magnitude greater than the lethal Gy-scale doses (10 J kg^{-1}) associated with nuclear disasters [3]. Thus, electron beam-induced radiolytic damage has long been heralded as the "fundamental limit" [4] constraining fields such as single-particle analysis [5], cryo-electron tomography [6], and electron crystallography [7].

Despite its crucial impact, little is known about the onset and progression of radiolysis in beam-sensitive molecular crystals. In electron crystallography, the primary metric used for assessing the extent of degradation induced by radiolysis is the disappearance of Bragg reflections in electron diffraction patterns [8]. Several previous studies have analyzed the radiolytic decay of Bragg reflections in organic and biomolecular crystals [9-12]. Critically, however, the scope of these analyses has mostly been limited to indirect observation via the back focal plane, and little is known about the concomitant changes in real space which *drive* the deterioration of Bragg peaks. Since accurate measurement of Bragg peak intensities is a key prerequisite to *ab initio* structure determination, a deeper understanding of radiolytic decay in molecular crystals is desired. Nevertheless, a *simultaneous* visualization of the effects of electron beam-induced radiolysis—in both real space and reciprocal space—remains elusive.

Here we apply low-dose scanning nanobeam electron diffraction [13, 14] to record simultaneous dual-space snapshots of organic and organometallic nanocrystals at sequential stages of beam-induced radiolytic decay. We show that the underlying mosaic of coherently diffracting zones (CDZs) continuously undergoes spatial reorientation as a function of accumulating electron exposure, causing the intensities of many Bragg reflections to fade nonmonotonically (Figure 1). Furthermore, we demonstrate that repeated irradiation at a single probe position leads to the concentric propagation of radiolytic damage well beyond the initial point of impact. These results sharpen our understanding of molecular crystals as conglomerates of CDZs whose complex lattice structure deteriorates through a series of dynamic internal changes during illumination. [15]

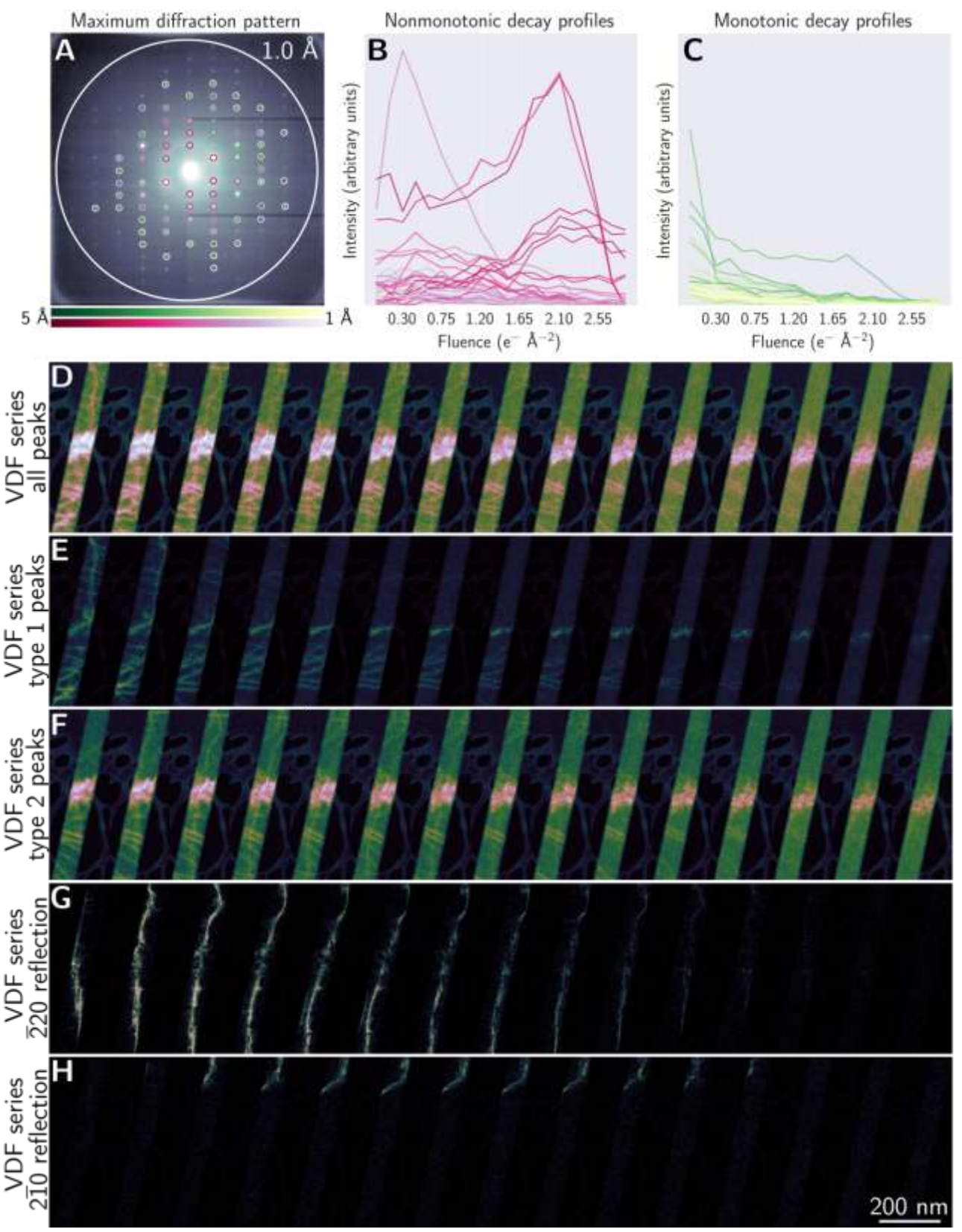
Maximum diffraction pattern
A
1.0 Å
5 Å
1 Å
Nonmonotonic decay profiles
B
Intensity (arbitrary units)
0.30 0.75 1.20 1.65 2.10 2.55
Fluence (e⁻ Å⁻²)
Monotonic decay profiles
C
Intensity (arbitrary units)
0.30 0.75 1.20 1.65 2.10 2.55
Fluence (e⁻ Å⁻²)
VDF series all peaks
D
VDF series type 1 peaks
E
VDF series type 2 peaks
F
VDF series $\bar{2}20$ reflection
G
VDF series $2\bar{1}0$ reflection
H
200 nm

Figure 1. Migration of coherently diffracting zones in biotin. (A) Maximum diffraction pattern across all scans in the time series. (B, C) Decay profiles of Bragg reflections undergoing (B) nonmonotonic (type 2) decay and (C) monotonic (type 1) decay, corresponding to the peaks encircled in (B) red and (C) green in (A). (D-H) Horizontal montages of VDF images reconstructed by placing reciprocal-space virtual apertures around (D) all 68 Bragg reflections identified in (A), (E) 38 Bragg reflections undergoing nonmonotonic decay, (F) 30 Bragg reflections undergoing monotonic decay, (G) a single Bragg reflection undergoing nonmonotonic decay which is present in the first scan and transiently grows stronger, and (H) a single Bragg reflection undergoing nonmonotonic decay which first appears in the third scan. Each VDF image represents a consecutive 4D-STEM experiment.

References

[1] K. Stenn and G. F. Bahr, *J. Ultrastructure Res.* 31, 526-550 (1970).
[2] R. Henderson, *Q. Rev. Biophys.* 28, 171–193 (1995).
[3] V. Drozdovitch, *Frontiers in Endocrinology* 11 (2021).
[4] L. A. Baker and J. L. Rubinstein, in *Methods in Enzymology*, Vol. 481, edited by G. J. Jensen (Academic Press, 2010) pp. 371– 388.
[5] Y. Cheng, N. Grigorieff, P. A. Penczek, and T. Walz, *Cell* 161, 438–449 (2015).
[6] M. Turk and W. Baumeister, *FEBS Letters* 594, 3243–3261 (2020).
[7] A. Saha, S. S. Nia, and J. A. Rodriguez, *Chem. Rev*., 122, 13883–13914 (2022).
[8] R. M. Glaeser, *J. Ultrastructure Res.* 36, 466–482 (1971).
[9] L. Reimer and J. Spruth, *Ultramicroscopy* 10, 199–210 (1982).
[10] P. Li and R. F. Egerton, *Ultramicroscopy* 101, 161–172 (2004).
[11] M. J. Peet, R. Henderson, and C. J. Russo, *Ultramicroscopy* 203, 125–131 (2019).
[12] K. Naydenova *et al*., *Ultramicroscopy* 237, 113512 (2022).
[13] K. C. Bustillo *et al*., *Acc. Chem. Res.* 54, 2543–2551 (2021).
[14] M. Gallagher-Jones *et al*., *Comm. Biol.* 2, 1–8 (2019).

[15] Work at the Molecular Foundry was supported by the Office of Science, Office of Basic Energy Sciences, of the U.S. Department of Energy under Contract No. DE-AC02-05CH11231. This research used resources of the National Energy Research Scientific Computing Center (NERSC), a U.S. Department of Energy Office of Science user facility located at Lawrence Berkeley National Laboratory, operated under Contract No. DE-AC02-05CH11231.